UILU-ENG-87-2001

CIVIL ENGINEERING STUDIES

STRUCTURAL RESEARCH SERIES NO. 531

ISSN: 0069-4274

3-DIMENSIONAL CONTRIBUTION TO FRAME-WALL LATERAL BEHAVIOR

By
CLAUDIO CHESI
and
W. C. SCHNOBRICH

A Report on a Research Project
Sponsored by
THE NATIONAL SCIENCE FOUNDATION
Research Grant CEE 83-12041

DEPARTMENT OF CIVIL ENGINEERING
UNIVERSITY OF ILLINOIS
AT URBANA-CHAMPAIGN
URBANA, ILLINOIS
FEBRUARY 1987

50272-101

REPORT DOCUMENTATION PAGE	1. REPORT NO.	2.	3. Recipient's Accession No.

4. Title and Subtitle
3-Dimensional Contribution to Frame-Wall Lateral Behavior

5. Report Date
February 1987

6.

7. Author(s)
Claudio Chesi and William C. Schnobrich

8. Performing Organization Rept. No.

9. Performing Organization Name and Address

University of Illinois
208 North Romine Street
Urbana, IL 61801

10. Project/Task/Work Unit No.

11. Contract(C) or Grant(G) No.
(C) CEE 83-12041
(G)

12. Sponsoring Organization Name and Address

National Science Foundation
1800 "G" Street, NW
Washington, D.C. 20550

13. Type of Report & Period Covered

14.

15. Supplementary Notes

16. Abstract (Limit: 200 words)

Behavior of the first floor of the U.S.-Japan seven story reinforced concrete test structure was modeled by a finite element model. The constitutive matrix describing material behavior is a normal concrete model which included a smeared cracking capability. The computed response of the system was shown to have a dependence on the level of tension stiffening present in the concrete. The selection too low a value distorted the behavior observed in the model. The 3-dimensional effects presented in the test structure was also observed in the computational model. Motion of the tension column was transmitted through the slab and beams to the outer frames. This mechanism provided a significant contribution to the lateral load resistance.

17. Document Analysis a. Descriptors

Earthquake Response, Full-Scal: Test, Inelastic Behavior, Finite Element Analysis

b. Identifiers/Open-Ended Terms

c. COSATI Field/Group

18. Availability Statement	19. Security Class (This Report) Unclassified	21. No. of Pages 41
	20. Security Class (This Page) Unclassified	22. Price

(See ANSI-Z39.18) *See Instructions on Reverse* OPTIONAL FORM 272 (4-77)
(Formerly NTIS-35)
Department of Commerce

3-DIMENSIONAL CONTRIBUTION TO FRAME-WALL LATERAL BEHAVIOR

by

Claudio Chesi
and
W. C. Schnobrich

A Report on a Research Project
Sponsored by the
National Science Foundation
Research Grant CEE 83-12041

University of Illinois at Urbana-Champaign
Urbana, Illinois

February 1987

TABLE OF CONTENTS

3-DIMENSIONAL CONTRIBUTION TO FRAME-WALL LATERAL BEHAVIOR

by Claudio Chesi and William Schnobrich

INTRODUCTION

The subject of the research was suggested by the U.S.-Japan Cooperative Research Program, which consisted of the construction and pseudo-dynamic testing of a model building. In that program, the test specimen was a full-scale seven-story reinforced concrete frame-wall structure. Figs. 1 and 2 show schematic views of that structure. Resistance to lateral loads was provided by three parallel frames: two moment resisting space frames (the outer ones, frames A and C) and a coupled frame-wall (frame B). The connection among frames was realized by floor slabs with transversal beams.

Several interesting aspects of the seismic behavior of concrete frames have been clarified by the experimental work and subsequent analytical studies associated with the NSF supported research being performed within that program. In this investigation, interest has been devoted to a specific experimental result, showing the sort of interaction occurring among parallel frames, due to the coupling action of transversal beams.

In the early stages of loading, the response is controlled mainly by shear wall deformation. As loading proceeds, bending in the plane of the wall, indeed, causes extremely large elongation at the tension side of the wall, so that transversal beams framing into that wall undergo large relative vertical displacements between their ends. The shear forces thus generated have a stabilizing effect on the shear wall, increasing,

at the same time, the overturning moment in the outer frames. This is the so-called "3-dimensional effect."

The contribution of the 3-dimensional effects to the building's ultimate resistance has a simple but meaningful interpretation in a collapse analysis, assuming that in the collapse mechanism plastic hinges develop at all the transversal beam ends (Yoshimura and Kurose, 1985). More complete studies have been developed by Otani et al. (1985) and by Charney and Bertero (1982). These authors have incorporated the 3-dimensional effect into computer codes for frame analysis, by simply introducing spring connections between the shear wall tension side and the corresponding columns in the outer frames. The spring stiffness is taken as close as possible to the transversal beam stiffness.

In the present work, a finite element non-linear model is developed, representing a single floor of the test structure. The load has been progressively increased through a static monotonic process. Attention has been focused on the mechanisms generating the 3-dimensional effect. An estimation is also given of the contribution of this last mechanism to the total building resistance at different load levels.

NUMERICAL MODEL

The portion of the building included in the numerical model consisted of the first story plus a portion of the next story, up to mid-height between the first and second floor. Due to symmetry of the structure about the plane containing the shear wall, only one side, i.e., one-half of the building, was analyzed. A schematic view of the

structure as modelled is shown in Fig. 3; the finite element modelling of it resulted in the grid of Fig. 4.

The following two kinds of elements have been used for the discretization of the different structural components:

1) For the shear wall: a 9-node Lagrangian shell element (Milford and Schnobrich, 1984); the wall is subjected to in-plane forces only, so the element is used mainly to describe a membrane behavior.

2) For the slab: the same kind of shell element but here it is subjected to both in-plane and out-of-plane forces.

3) For the T-beams, resulting from an effective slab width plus eccentric web: the webs have been represented by the eccentric shell stiffener beam element (Milford and Schnobrich, 1984), which is in the form of a 3-node Lagrangian beam element. This last element, if used in conjunction with the 9-node Lagrangian shell element, is expected to provide an accurate description of the T-beam behavior. This feature was of special interest for the present analysis, as there was experimental evidence of a beam-slab interaction having a much more pronounced effect than conventionally assumed.

4) For the columns: the same elements as in 3), which can simply work as beam column elements, if not coupled to shell elements.

5) For the shear wall's eccentric columns: again, the same beam elements as in 4), but now with a zero bending stiffness.

Non-linear material behavior was specified for all the elements but the columns. In the Milford and Schnobrich formulation, the beam is handled as a layered system, thus, the non-linear beam elements have non-zero bending stiffness in one direction only. For the purpose of

analyzing the 3-dimensional effect, however, bi-axial column bending had to be considered for the columns in the outer frames. These columns were, thus, considered to remain elastic. This assumption of elastic behavior for columns is supported by experimental results, those results showing plastic hinges occurring in beams much earlier than in columns.

The RCSHELL and RCBEAM material models (Milford and Schnobrich, 1984) present in Finite for the analysis of non-linear analysis of concrete behavior have been used in this study. Although these models represent exactly the same material, two distinct material specifications are required for shell and beam elements respectively. The concrete properties which are required as input to the material models are listed in Table 1 (see also Fig. 5). A reduced integration order (2x2 for shell elements and 2 for beam elements) has been used, so as to reduce possible problems from membrane and/or shear locking, the phenomena often observed with this class of element. With this implementation, no problems were encountered relative to the possible activation of zero-energy modes.

The unloading capabilities, as incorporated in the two material models, have been proven to be very important even for a monotonic loading process. As cracking is occurring at some integration points, indeed, temporary unloading and/or re-loading may be taking place at some other points. A typical σ-ε relationship as it will exist following several subsequent load steps is shown in Fig. 6 for a generic integration point. The tension stiffening parameter (β), governing the post-cracking behavior of concrete, has shown a remarkable effect on the global structural response. Figure 7 shows the crack distribution

recorded in the shear wall at collapse for the cases computed while using β=5 and that for β=20. The corresponding σ-ε relationships for the reinforced concrete in the shear wall and that in the end columns are shown in Fig. 8. In both cases (i.e., for the two β values) a shear collapse occurs, although the two mechanisms are quite different. Note that in the second case (β=5), the horizontal crack at the wall base has propagated to all the integration points along the lowest level, and the wall bending stiffness was consequently sensibly reduced.

In carrying out this investigation while using a model which includes only the first one and one-half stories, the following loads have been applied to the model:

- vertical load, including slab weight and axial loads on columns and shear wall; these represent the effects of the upper stories in the response;
- lateral load, including horizontal inertia force at the slab level, shear force and moment at the top of the wall.

The lateral load was affected by a multiplier, representing the ratio between the total horizontal force and the total building weight (referenced in the following as the "lateral load intensity factor").

The constraints imposed on the model are:

- symmetry conditions on the symmetry plane;
- fixed conditions at the column ends and shear wall bases;
- hinges at the column's mid-heights;
- the same horizontal displacement for the columns and the shear wall at the top of the model.

Moreover, the same z rotation (see Fig. 4) is imposed at all of the nodes at the slab-wall intersection; this stipulation is required as a consequence of the absence of a drilling mode for the planar wall elements. The theory which forms the basis for the development does not include a stiffness for rotations around the normal. This is a typical problem for shell elements intersecting at right angles.

Several different models (ten) had to be tried, before the proper one could be defined. Major difficulties originated from two problems:

1) In the early attempts to solve the problem, the model included a generic floor, with the shear wall and columns spanning one-half of the interstory height above and below the slab. In this way, the modelled portion of the wall was 5 m (16'5") wide and 3 m (10') high. The constraints associated with the model make it impossible for the expected bending behavior to develop. By analyzing a model which included the entire first story, instead, (i.e., from the base of the columns to mid-height between the first and second stories) allowed the inclusion in the model of a larger portion of the wall. The expected behavior was then observed.

2) Special care had to be used in the definition of the normal and the shear stresses applied at the top of the shear wall. These represent the shear load and moment coming from the upper structure. Improper stress distributions caused a local failure before a global collapse of the model could take place. The solution shown in Fig. 9 was then adopted: an extra portion of the wall was included in the model and the loads applied at the top of that wall. In this way, the same moment at the base of wall could

be developed by lower intensity forces. Stresses, moreover, were not imposed in the whole region of interest but, rather, were allowed to redistribute.

Note also that a simplified model was used in most of the preliminary analyses, with non-linearity restricted to only the wall. This last, indeed, due to the extremely high lateral stiffness just of the wall itself, governs totally the model's global response.

A few remarks about the model:

1) The real structural behavior cannot be reproduced by a numerical model that includes only one floor:
   - not only external forces, but internal forces as well have to be specified, in order to represent continuity with upper floors. Internal forces, however, are not known a priori;
   - a single load pattern must be used throughout the analysis, while the internal force distribution depends on the load level;
   - due to the absence of the upper floors, column and wall axial loads representing those upper floors do not include the effect of the shear forces associated with the transverse beam bending of the upper levels.
2) As a consequence, the lateral load systems in the model and in the test structure are different. Equivalence between the two has been imposed so that yielding of the wall's main reinforcement occurs for the same lateral load factor in both cases.

3) It is worth underlining, however, that the model does not have, as its purpose, the reproduction of the global structural behavior; rather, it aims at reproducing the three-dimensional resistance contribution developed by the slab and transverse beams. This is a local phenomenon, requiring the analysis of a single floor only.

NON-LINEAR STATIC ANALYSIS - MAIN RESULTS

The non-linear analysis was carried out by progressively increasing the lateral load intensity factor through 136 load steps. Major efforts (see Appendix) were required to follow the crack opening and propagation throughout the shear wall, which governed the whole structural response. On the one side, indeed, the non-linear problem connected with wall cracking is a hard one. The wall is subjected to in-plane or membrane forces only. The stiffness contribution associated with an integration point suddenly drops to zero at that integration point as cracking occurs, then large amounts of load are released and have to be redistributed. On the other end, the shear wall is by far the stiffest element in the model, so that most of the lateral load is carried by it, and the resistance contribution from the other elements is very small.

The following is a brief history of the wall cracking and structural behavior.

The linear elastic range extends up to a lateral load intensity factor of 0.113 (note that, according to Wight et al. (1984), the design value was 0.112). Non-linearity occurs because of cracking at the base of the wall with the end column in tension (see Fig. 10). As a consequence of this, cracking soon extends to the adjacent points along

the wall base. During the next load steps, other points on the wall end column crack, followed immediately by the adjacent wall points. At the same time, the crack at the wall base propagates towards the compressed end, causing a "neutral axis migration" to take place. Note that, because of this last phenomenon, the increase in the moment is carried more by a lever arm action than by an increase in tension stresses. Figure 11 gives a clear picture of this effect; the increase of axial load in the column does not counterbalance that in the wall moment. At load step no. 84, the wall base and the end column are completely cracked (26 cracks opened or integration points cracked, see Fig. 10); then, the axial load in the left end column starts increasing again, until reinforcement yielding occurs in the end column at load step no. 119. This step corresponds to a lateral load factor of 0.244. The corresponding crack distribution is given in Fig. 10. The strain profile over a cross section at the base of the wall is shown in Fig. 12. Agreement with the experimental profile is satisfactory; note, moreover, that a few wall bars had already yielded at previous load steps.

The analysis was then carried on for a few more load steps, and terminated at load step no. 136, before the model had reached a complete collapse (no plastic hinges had formed yet in beams). The reason for stopping the analysis was due to the very low convergence rate of the model. The lateral load carrying capacity of the system, indeed, was extremely reduced, so that the load step size was necessarily very small. Most of the expected behavior had already developed.

A global description of the structural response is given in Fig. 13, in terms of the lateral load-horizontal deflection curve.

Sudden, but temporary decreases in stiffness can be observed at the cracking of each of the integration points of the wall end column in tension. The figure also shows the high degradation of the wall's lateral stiffness, resulting in the transfer of the additional shear forces from going into the wall to going into the adjacent columns, as the lateral load increases.

In order to investigate the 3-dimensional effect, attention has been focused on the elongation of the tension side of the wall, which is the key parameter controlling the bending of the transverse beams. With the cracks opening to nearly the compression column, the wall tends to pivot around that compression column. Thus, movement on the tension side is quite significant, while on the compression side the movements are nominal. Figure 14 shows the load deflection curve, relating the lateral load factor to the vertical displacements at the joint where the beams frame into the wall's tension side. The same behavior observed in Fig. 13 is reflected in this figure. A comparison is also given with test results. The model appears a little stiffer than the test structure, mainly at the low load levels (where the model assumes concrete to be uncracked).

The magnitude of vertical displacements suggests that bending of transversal beams has been activated. This is discussed in the following.

Figure 15 shows the axial loads present at the base of both the columns and the shear wall for a lateral load factor of 0.244. The effect of gravity is not included in the values given in Fig. 15. Columns A and C, connected by beams to the wall's tension side, undergo

much higher loads than the corresponding columns connected to the wall's compression side (as expected based on the observed displacements described in the previous paragraph). The effect is most pronounced in column C; the increase in axial load (ΔN_C), which comes from the transversal beam shear, gives a measure of the 3-dimensional effect. Figure 16 shows that, as expected, the axial load increase in the column and the shear in the transversal beam are about the same and grow proportionally to wall elongations. Note that the vertical equilibrium is satisfied by axial forces in columns A, B, C, D, E, and F. A portion of the boundary column's axial load has been transferred to the surrounding columns as a consequence of the wall's tension side elongation. The wall moment resistance is thus enhanced by the formation of a moment resisting mechanism, including both the wall and the columns.

A measure of the contribution developed by the 3-dimensional effect to the total resistance can be defined by comparing the moment developed by ΔN_C to the total overturning moment. The result of this comparison is shown in Fig. 17, where the beams at all the floors are supposed to develop the same contribution at collapse. Again, the dependence on the end column elongation is evident. After this member has entirely cracked, the percent contribution becomes almost constant. Note that a meaningful value of this is reached with the wall main reinforcement still elastic: the deformations activating the 3-dimensional effect come more from the concrete cracking than from column bar yielding.

The 3-D contribution to resist the overturning moment reached a value of 6.12% at load step no. 136, at which point the analysis was terminated. It is not difficult to give an approximate evaluation of

the maximum value for this 3-D contribution. A further increase of the lateral load would produce plastic elongation of the reinforcement in the wall's end column and formation of plastic hinges at both ends of the transverse beams (this was observed in the experimental analysis as well). In such a situation, the limit value for shear in transversal beams has been estimated as T = 6t (metric tons), or 13.2 kips, corresponding to a value of 6.87% for the above percentage contribution. (The average value of the shear stress in the transverse beam is about 5 kg/cm^2, or 70 psi.) This result is not far from the one given by Yoshimura (1985), who estimated the contribution of the transverse beams to building moment resistance at a value of 8%.

It is worth mentioning also that a meaningful contribution to the bending resistance of the transverse beams is provided by the slab. Clear evidence of this was given, among others, by Yoshimura (1985), through an analysis of the status of bar yielding in the test structure, and by Joglekar et al. (1985), who tested beam-column-slab assemblies. It is a common conclusion that the slab width which is effective with the beam in carrying moment is significantly larger than that prescribed by design codes (ACI 318-83 included). In the present analysis, eccentric shell stiffener beam elements have been used to model the transverse beams. This modelling allows a good representation of the beam-slab interaction phenomenon, and the same conclusion has been achieved.

Figure 18 shows bending moments in the transverse beams and both moments and tension strains in the slab, at load step no. 136. The slab contributes to the moment carrying capacity mainly by providing the beam with additional tension bars (the moment carried by the slab itself is

only a small percentage of total moment). In Fig. 18, a reasonable value for the effective slab width (w) is suggested (w is the ratio of total tension force carried by bars in the beam influence area and the tension per unit length at the beam axis). A value of w = 215 cm (7') is so found, while a value w = 150 cm (4'11") would be prescribed by the ACI 318-83 Code. When computing the limit value for the shear force, w = 215 cm was used. Note, however, that w is a function of the lateral load intensity (as also remarked by Joglekar et al. (1985)), in the sense that a higher value should be expected for higher load intensities.

CONCLUSIONS

The behavior of the first floor of the U.S.-Japan seven-story test structure was modelled by a finite element model, which used as its material, those properties of reinforced concrete. Nine-noded shell and three-noded beam elements were selected for the model.

The computed response of the system was shown to have a dependence on the level of tension stiffening assumed to be present in the concrete. Selection of too low a value for the stiffening parameter β distorts the behavior observed in the model. Values of 5 and 20 were used in this study.

The three-dimensional effects present in the test structure were also present in the model. With increased deflections the wall tended to pivot about the compression columns. The motion at the tension column was transmitted through the transverse beams to the columns in the out frames. Computed response was similar to the experiment.

The computed effective slab width was found to be in excess of that prescribed by ACI 318-83.

ACKNOWLEDGEMENTS

The work summarized in this report was performed by C. Chesi while he was on sabbatical from the Politecnico Di Milano. Support for this study was provided under the National Science Foundation Grant No. CEE 83-12041.

Concrete initial tangent modulus (E_o)	237000	kg/cm²
Concrete cylinder strength (f'_c)	290	"
Concrete tensile strength (f'_t) *	22	"
Strain at maximum concrete stress (ε_{cu})	0.0021	
Ultimate stress factor (FCU)	0.89	
Ultimate strain factor (ECU)	1.42	
Linear elastic option	"FALSE"	
Fixed crack direction option	"FALSE"	
Concrete tension stiffening	"TRUE"	
Concrete tension stiffening factor (β)	5	
Number of concrete layers	8	
Number of reinforcement layers	4	
Reinforcement tangent modulus	1710000	kg/cm²
Reinforcement plastic modulus	0	
Reinforcement tension stiffening	"FALSE"	
Yield stress of reinforcement	3650	kg/cm²

Then, for each reinforcement layer at each integration point:

- depth of reinforcement layer "i"
- area of reinforcement for layer "i"
- direction of reinforcement layer "i"

(*) Concrete tensile strength computed as:

$$f'_t = 5\sqrt{4200} = 324 \text{ psi} = 22 \text{ kg/cm}^2$$

TABLE 1

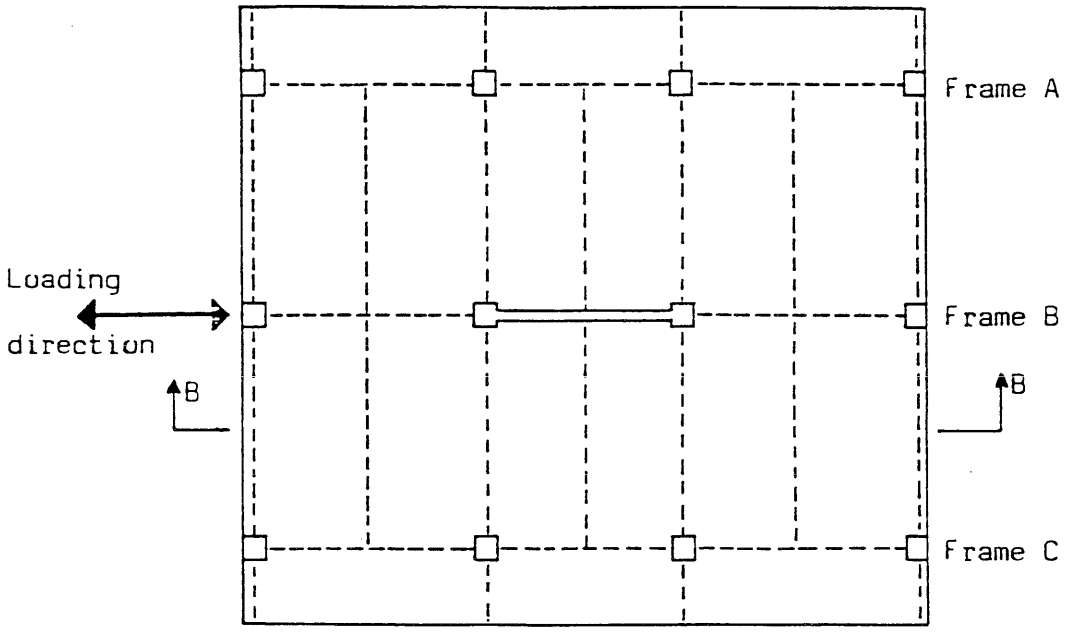

Figure 1 Test specimen (full-scale seven-story building): typical floor plan

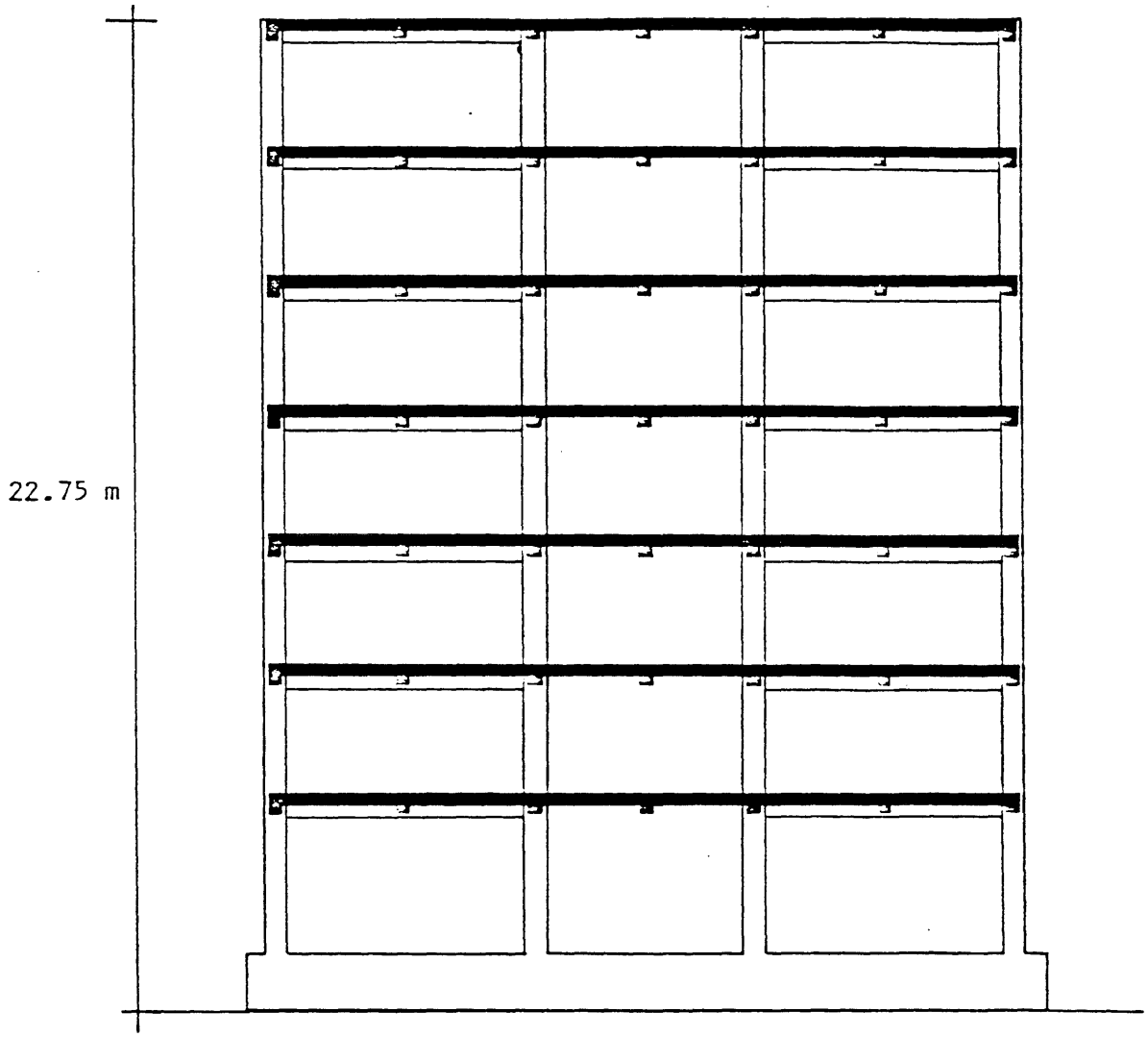

Section B-B of fig. 1

Figure 2 Test specimen: elevation

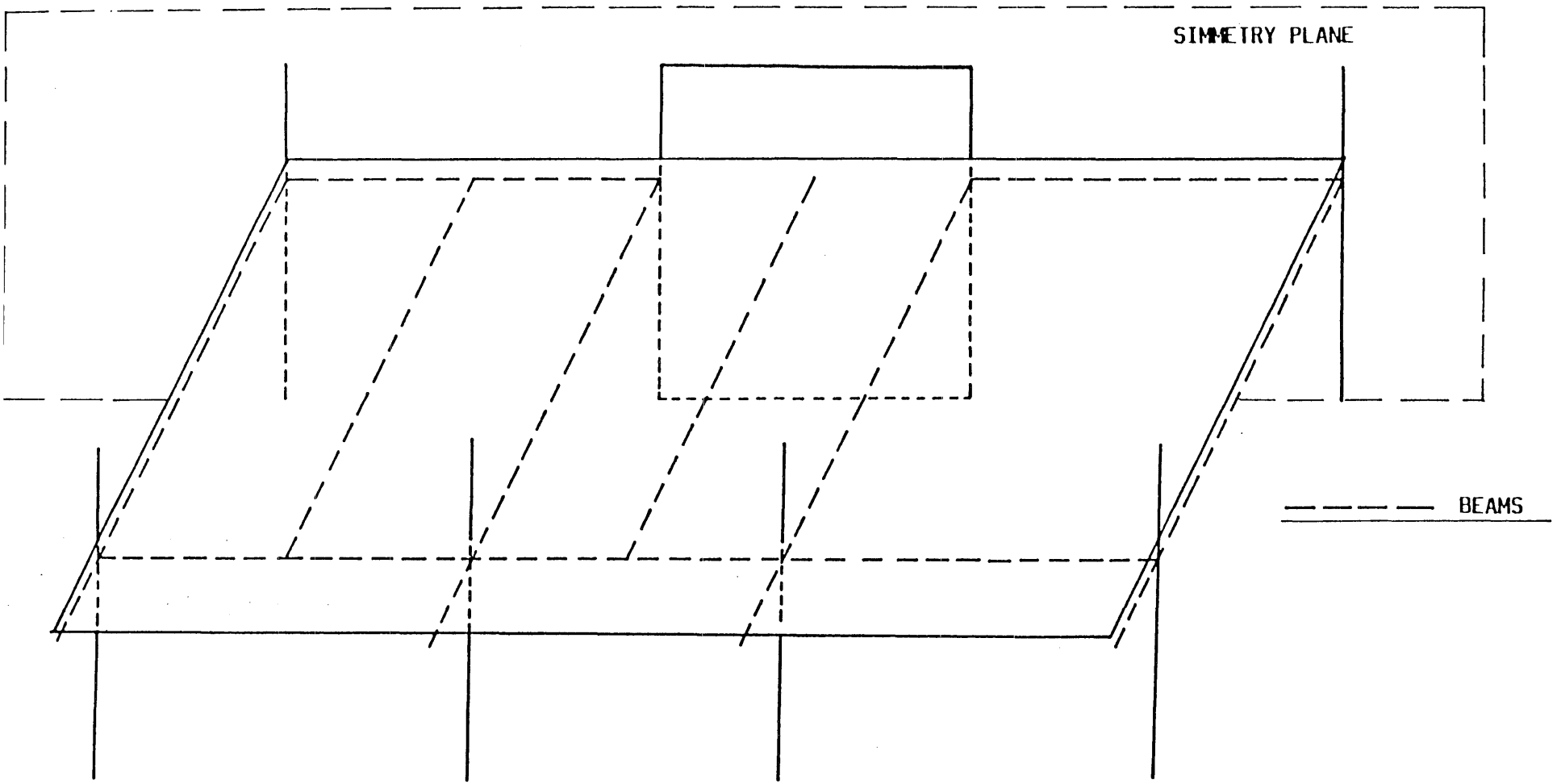

Figure 3 Test specimen: a schematic view of the portion of the building included in the numerical model

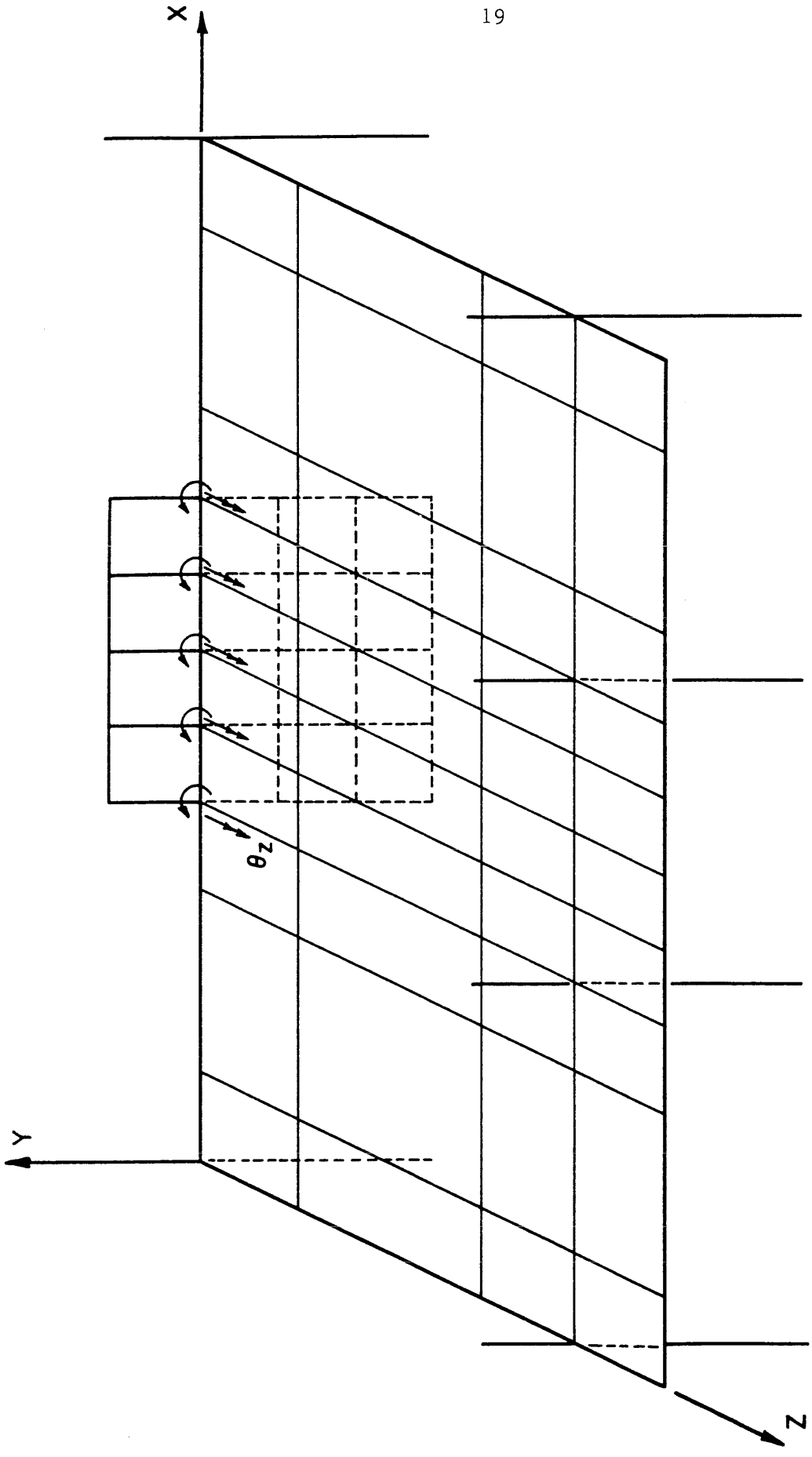

Figure 4 Finite element model: the grid

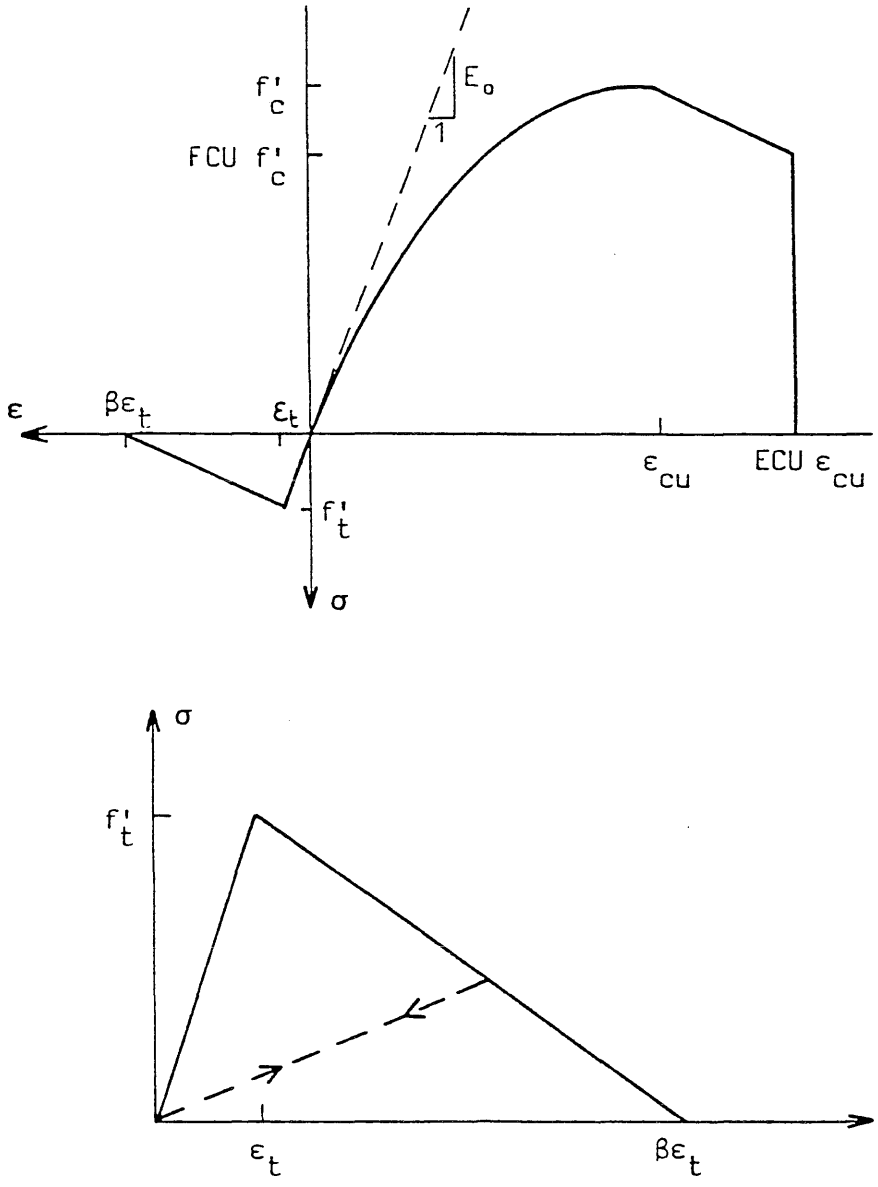

Figure 5 Stress strain relationship for concrete (a) and behavior of concrete in tension (b) with the TENSC option

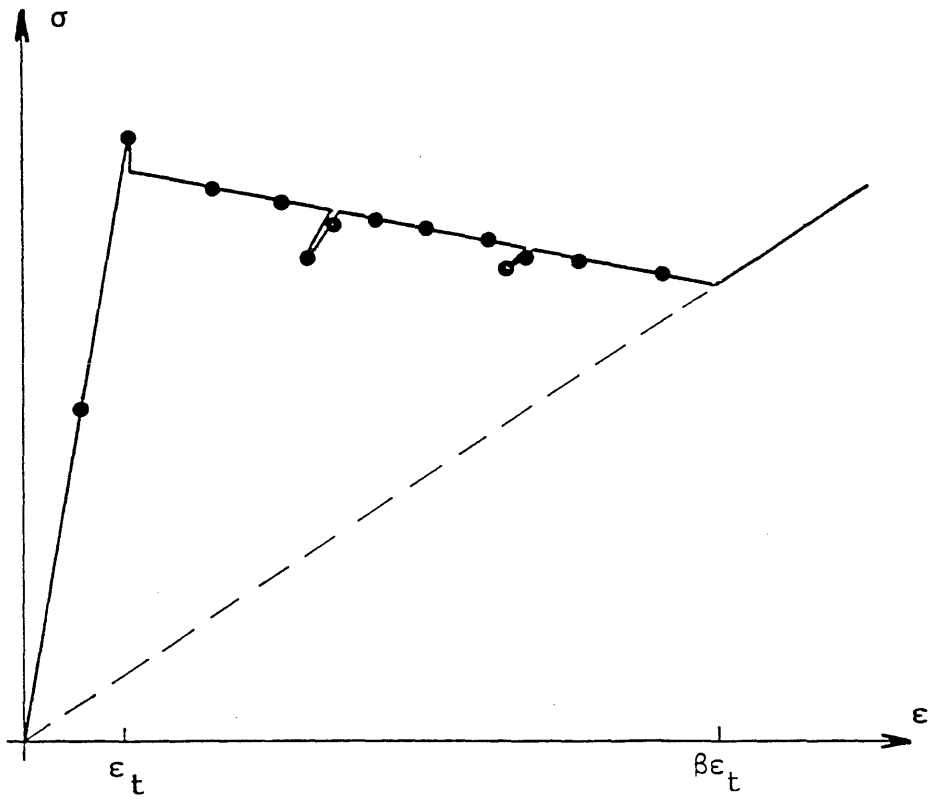

Figure 6 Typical unloading-and-reloading behavior of concrete in the softening range

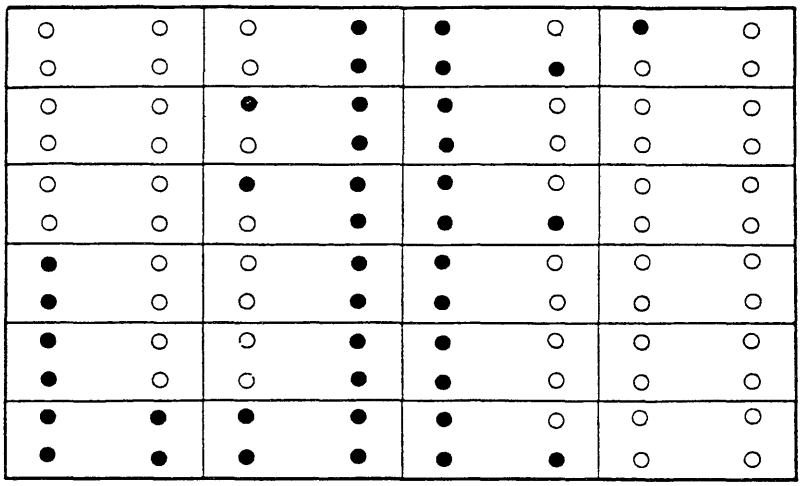

β = 20

● cracked concrete

○ uncracked concrete

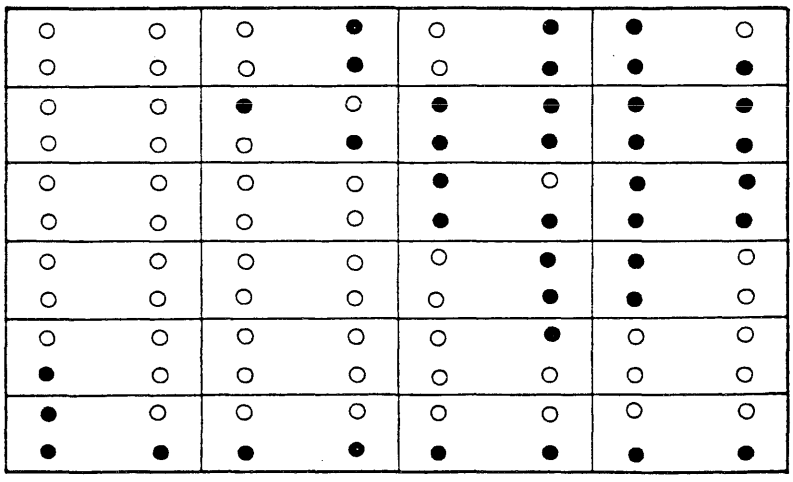

β = 5

Figure 7 Crack distribution in the shear wall for different values of the β parameter

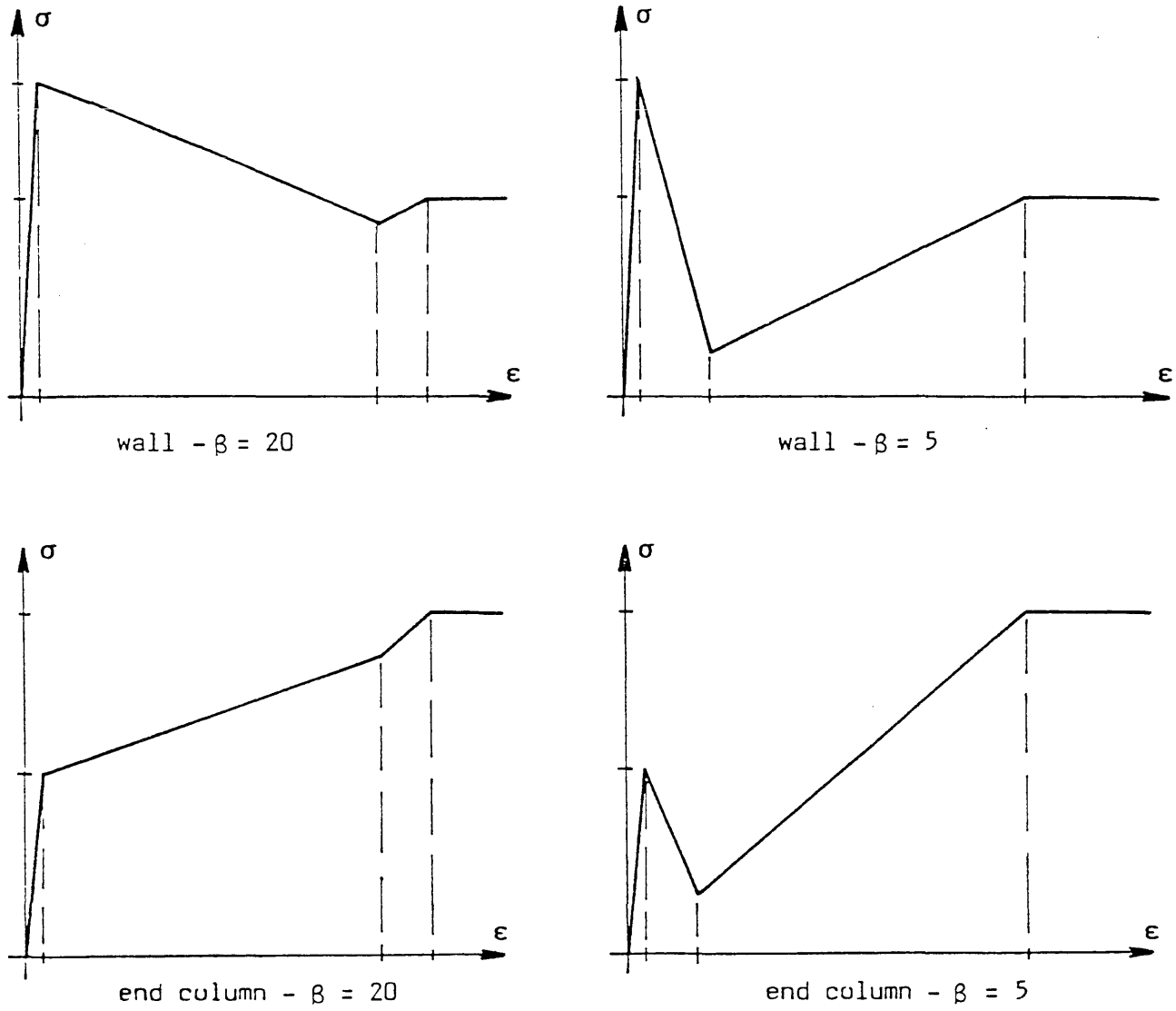

Figure 8 Stress strain relationships for reinforced concrete for different values of the β parameter

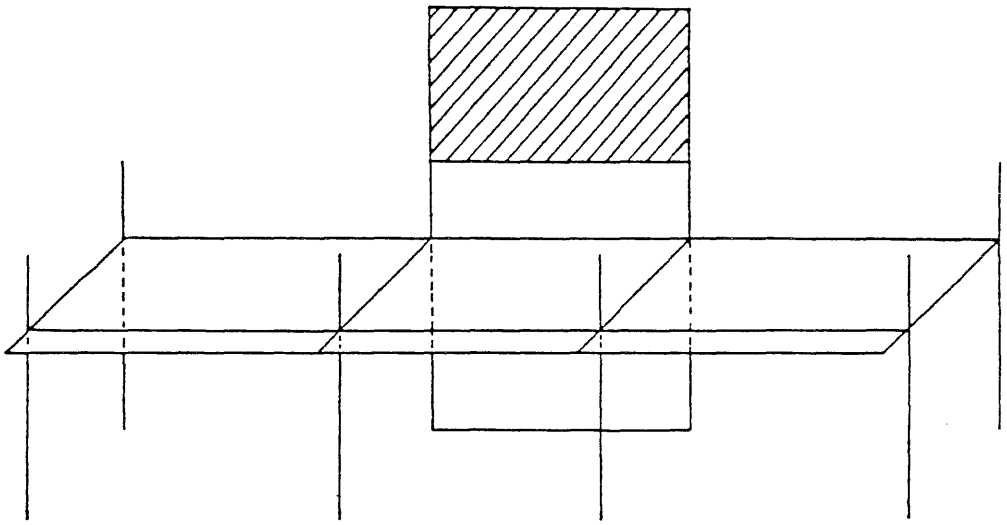

Figure 9 The modified scheme for the finite element analysis, including an extra-portion of the shear wall

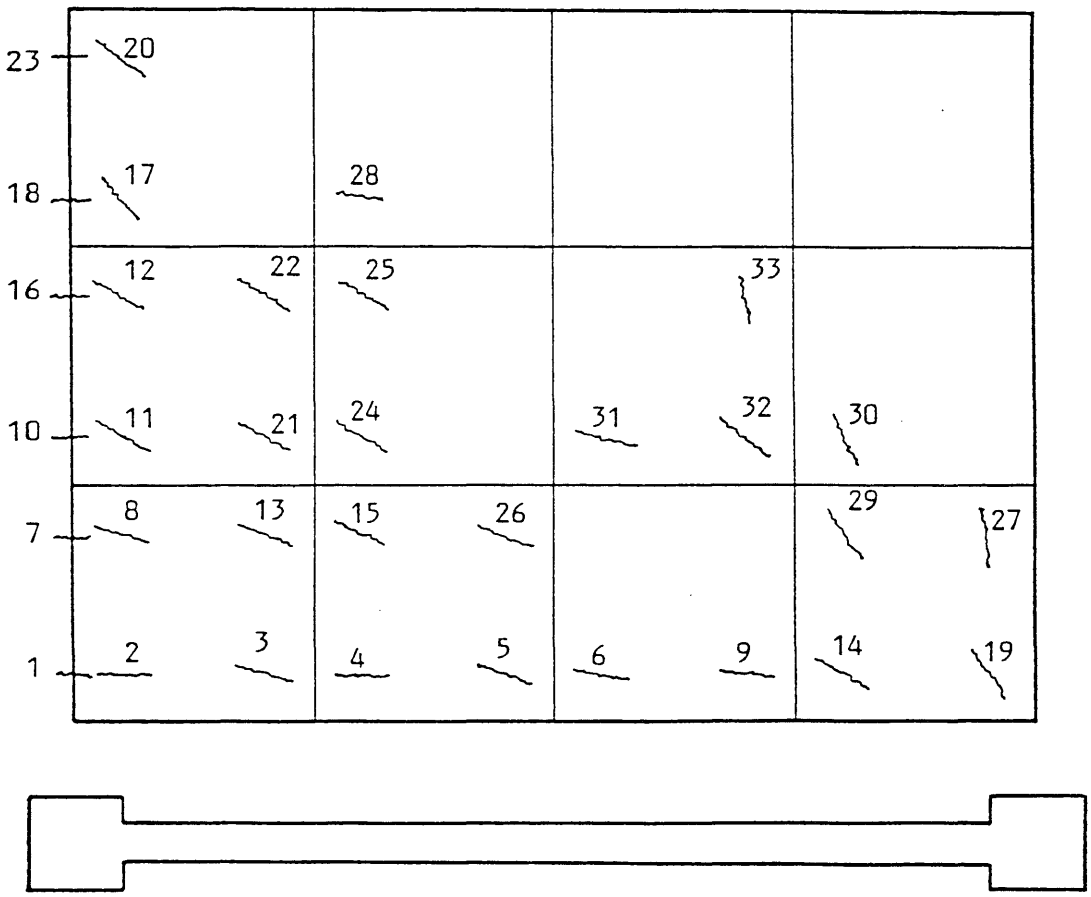

Figure 10 Crack distribution and orientation in the shear wall at yielding of reinforcement in the tension end column (load step n. 119). Numbers give the cracking sequence.

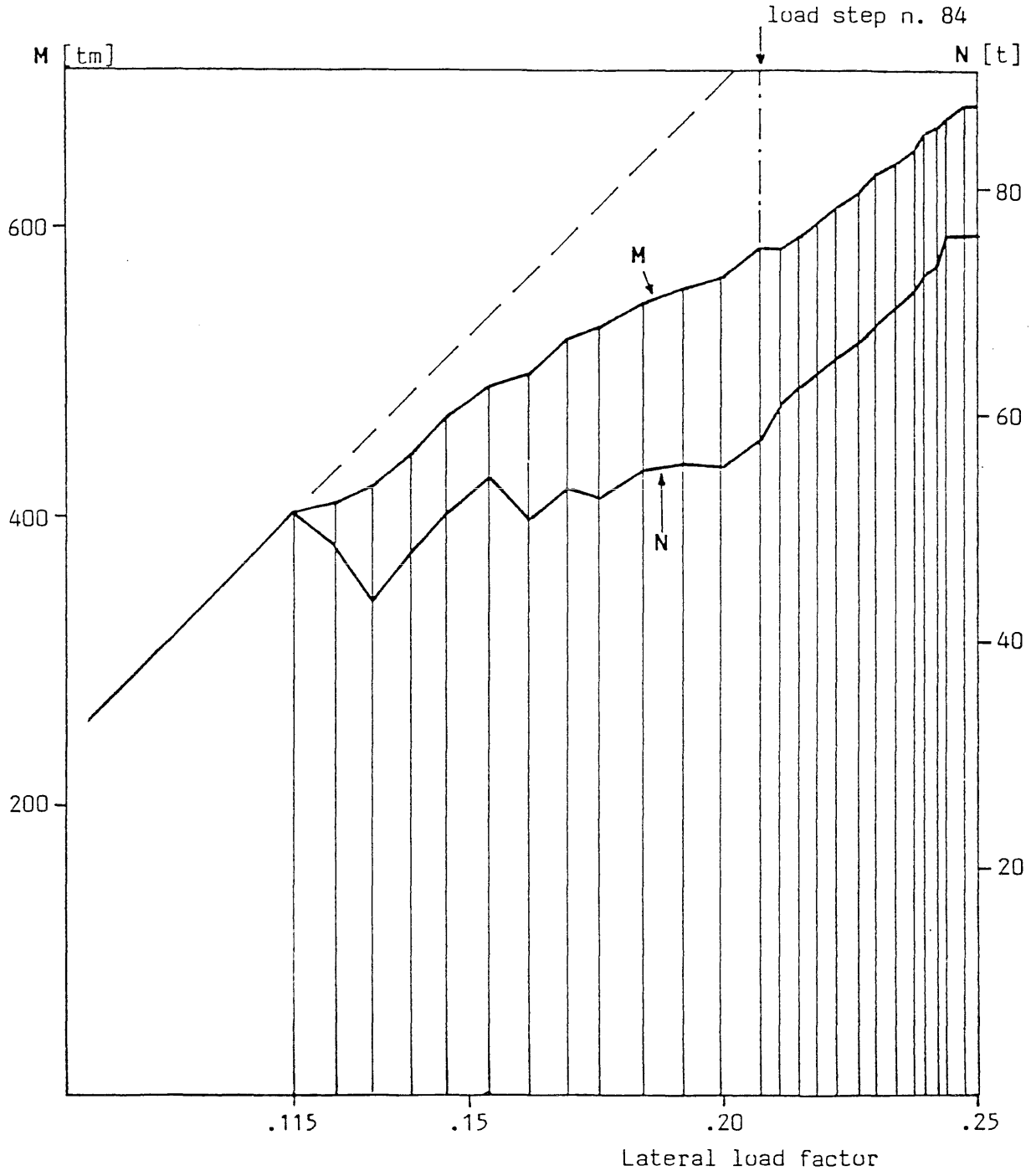

Figure 11 Variation of moment in the shear wall (M) and of axial load in the tension end column (N) during the load process

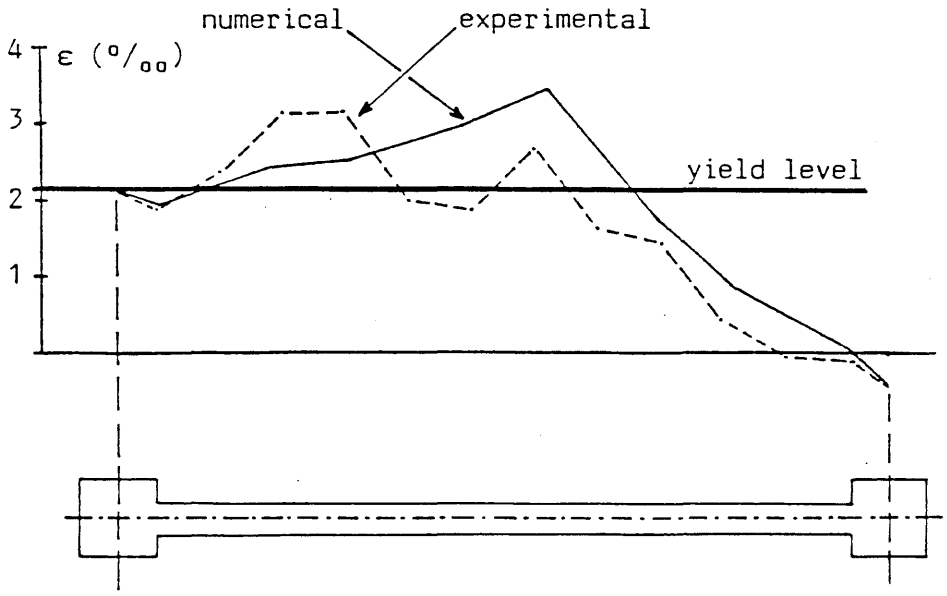

Figure 12 Vertical strain profile on the cross section at the wall base (load step n. 119)

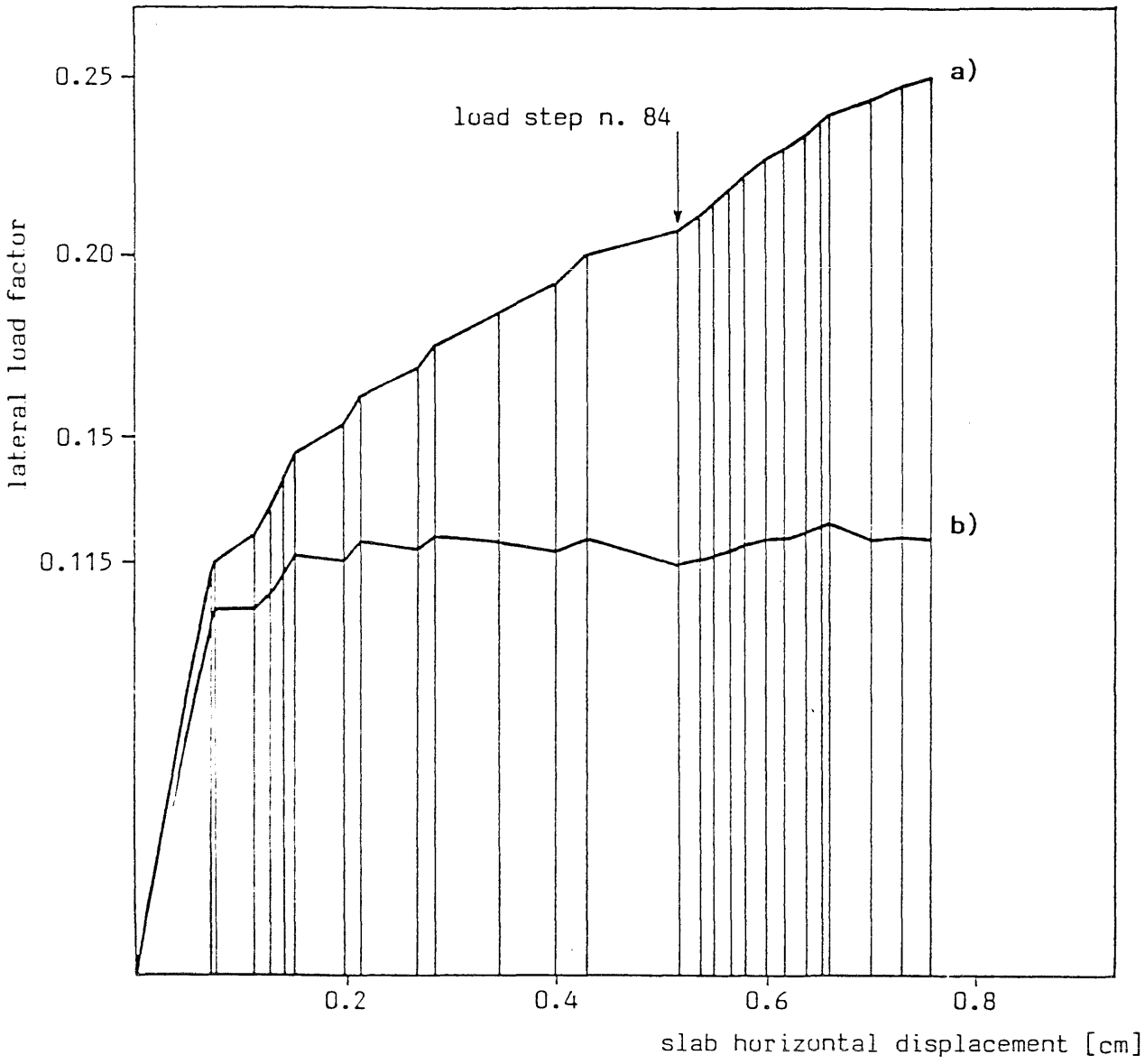

Figure 13 Lateral load factor versus the slab horizontal displacement: a) total base shear, b) wall base shear

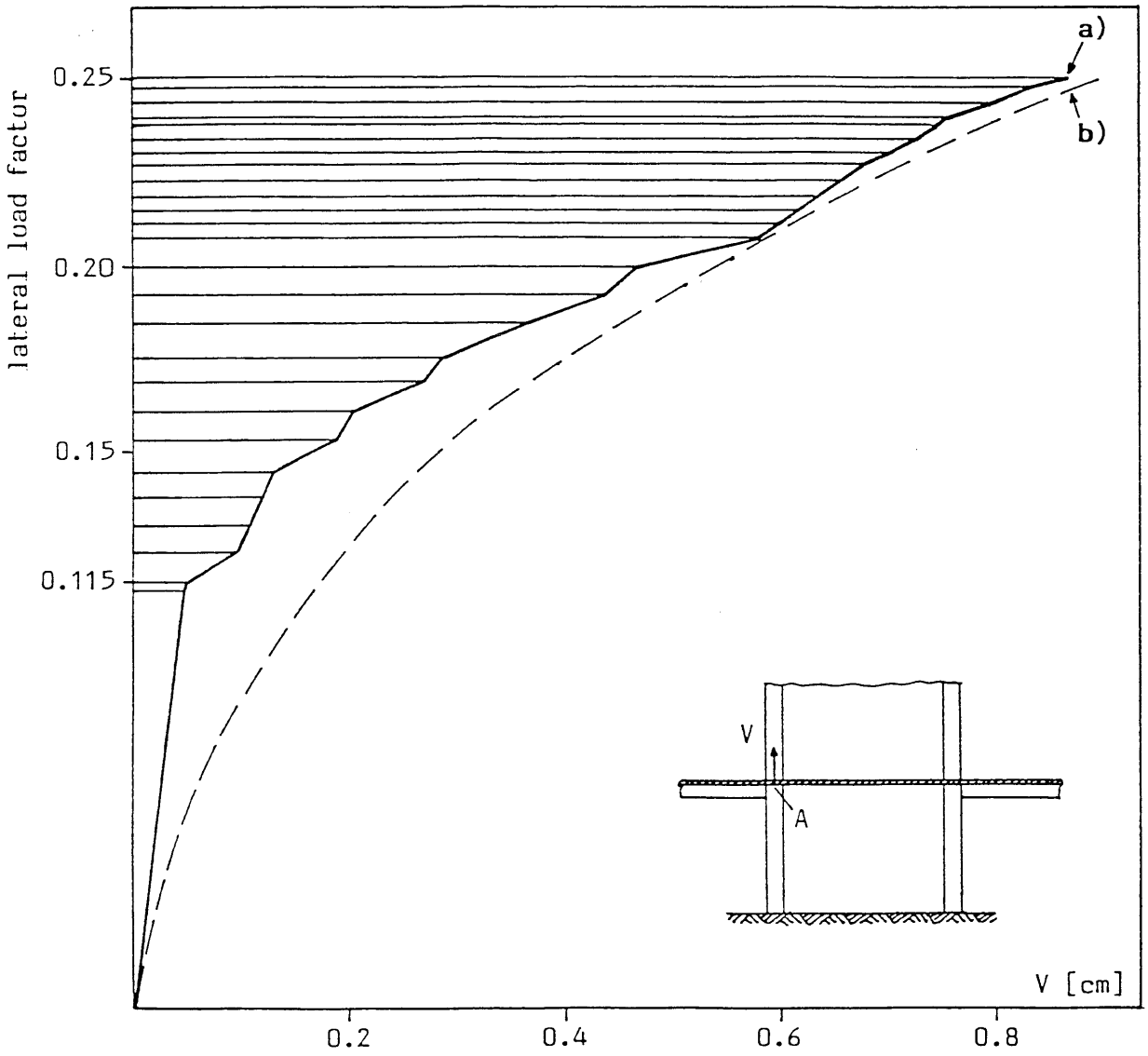

Figure 14 Lateral load factor versus the slab vertical displacement at point A. Numerical (a) and experimental (b) results.

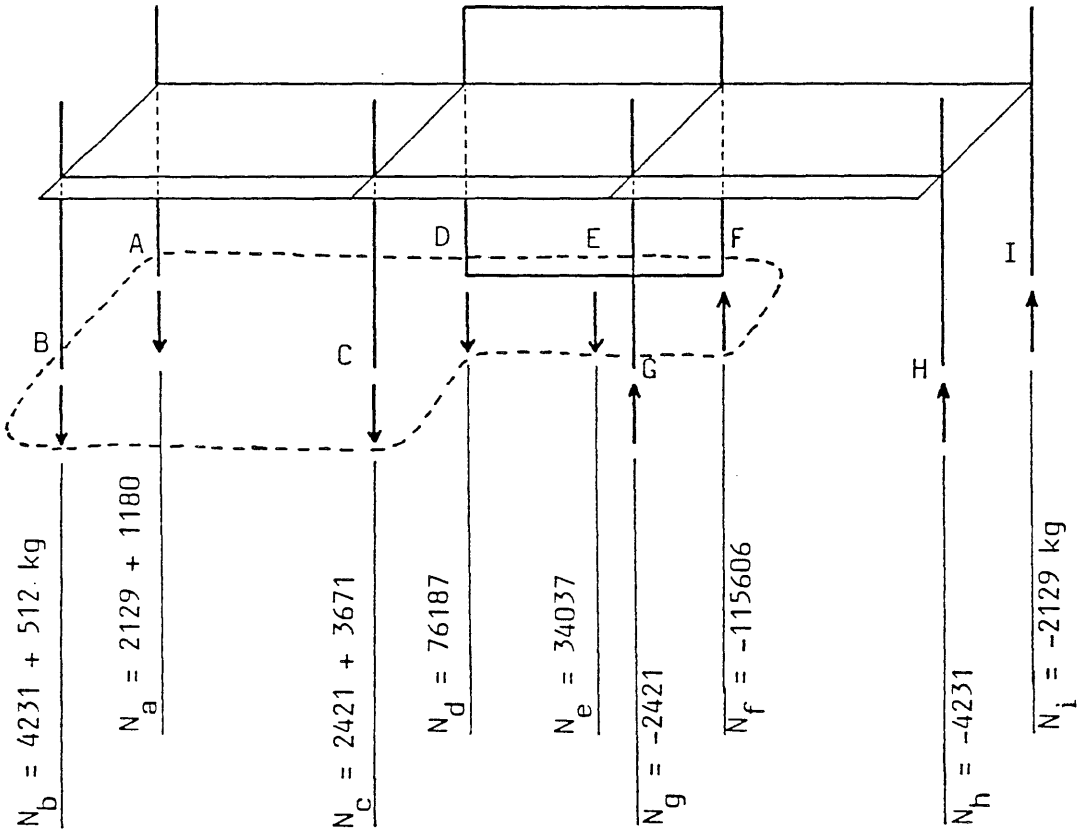

Figure 15 Axial loads at the base of columns and shear wall at load step n. 119 (lateral load factor = 0.244)

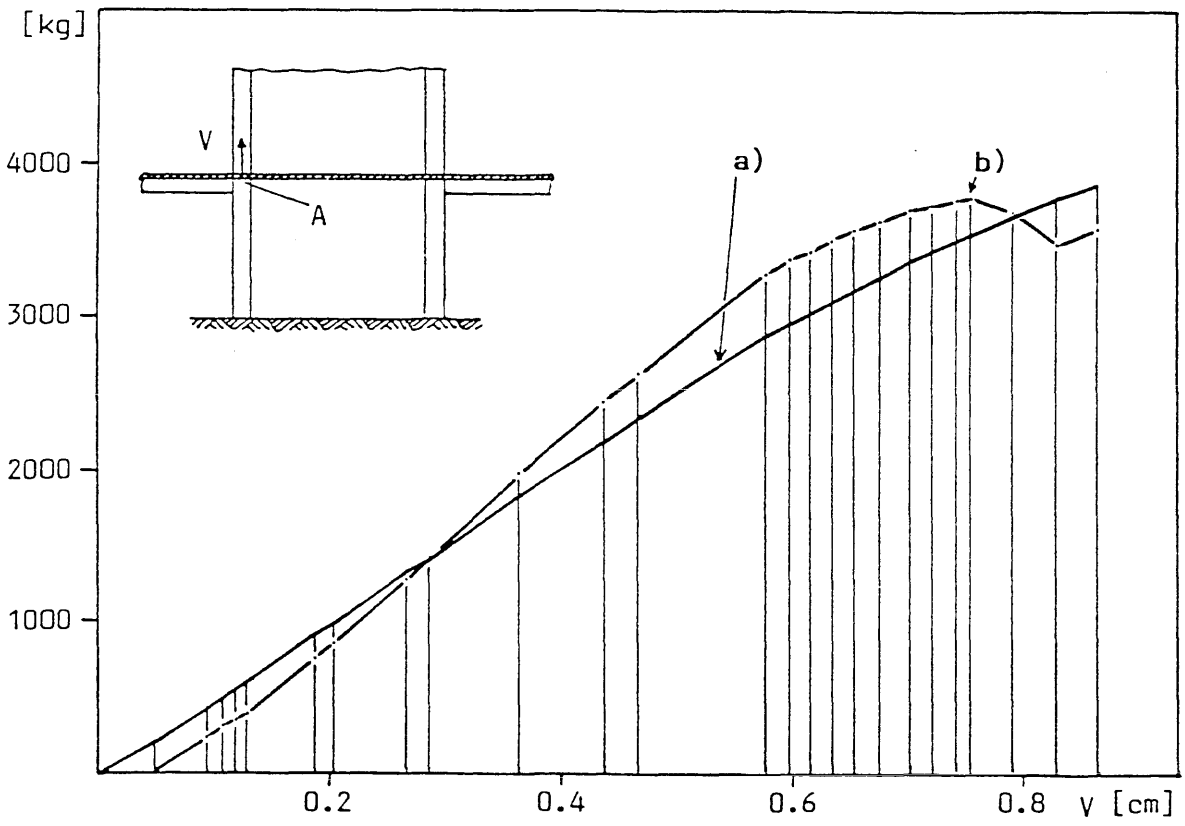

Figure 16 Variation of shear in the transversal beam (a) and axial load increase in column C (b) as a function of the vertical displacement at point A

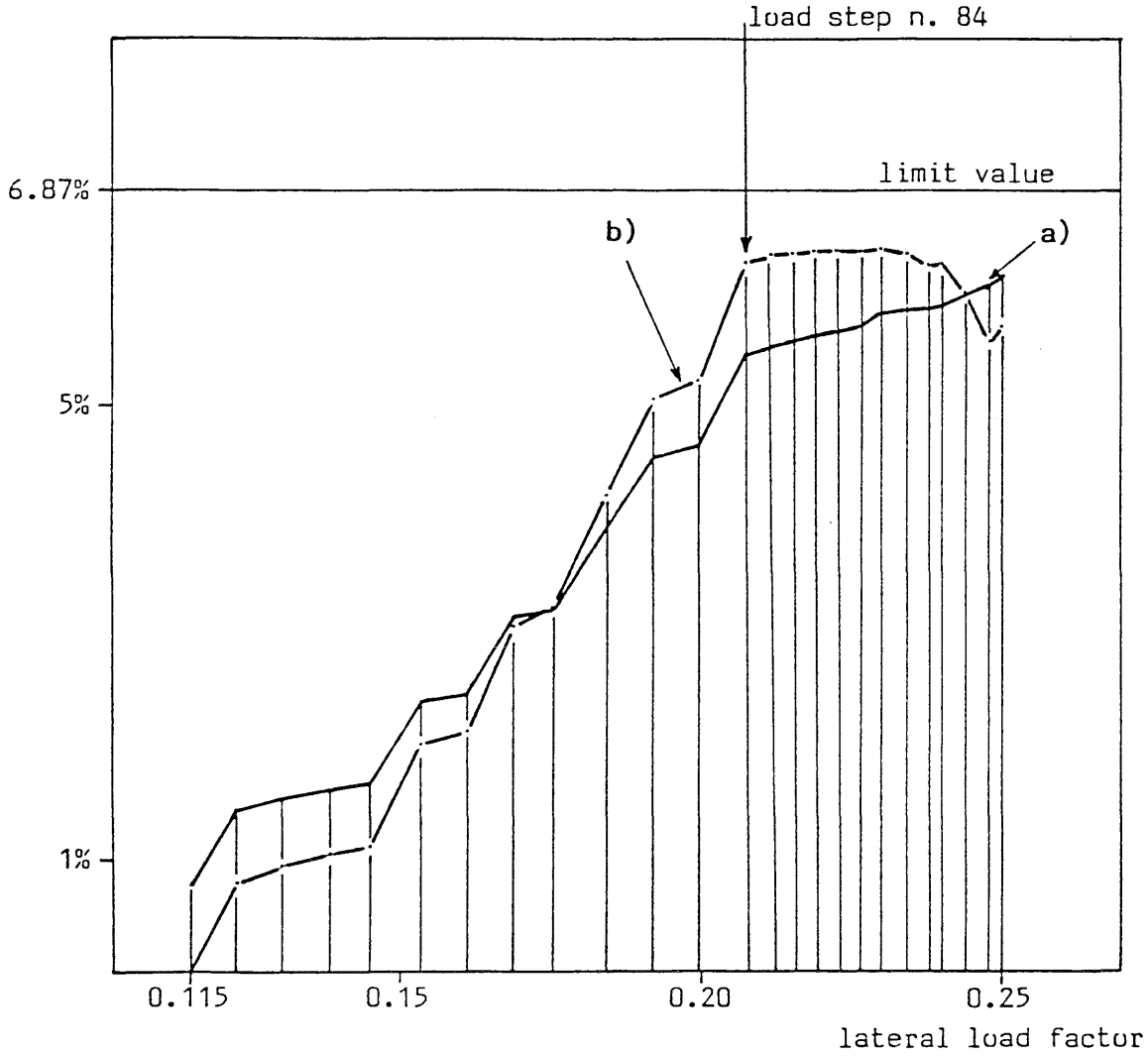

Figure 17 Percentage of the global overturning moment carried as 3-dimensional effect versus the lateral load factor. (a) Transversal beam shear; (b) axial load increase in column C.

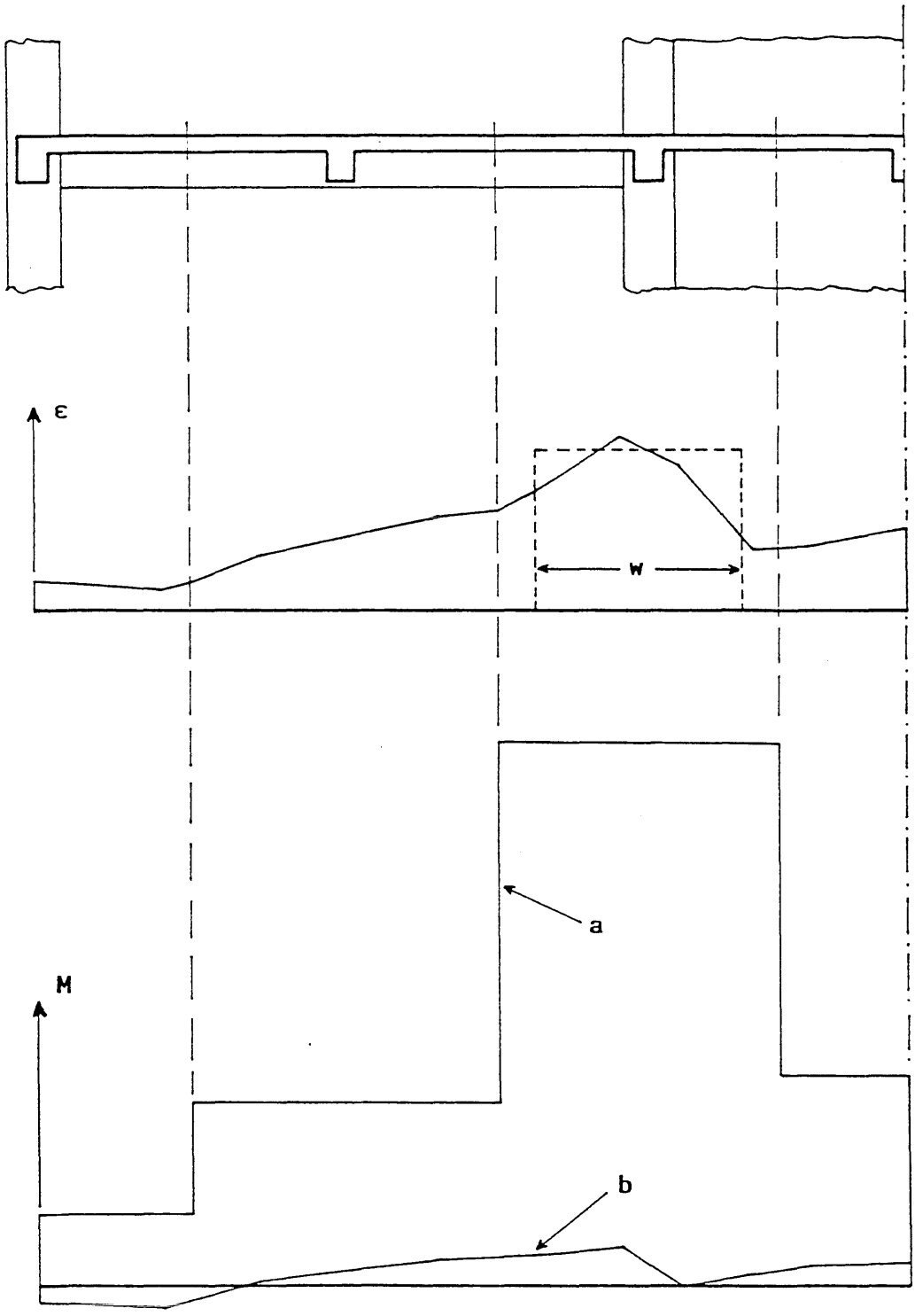

Figure 18 Bending moments for beams (a) and slab (b) and slab strains at the level of top reinforcement along a longitudinal section. The beam moments have been distributed on the beam influence widths.

APPENDIX

The RCSHELL and RCBEAM Material Models

Two options exist for handling the tension stiffening effect present in a finite element description of the behavior of a region of reinforced concrete: TENSC and TENSS. With TENSC the stiffening is assigned to the concrete model, while with TENSS the steel model reflects the stiffening effect.

1) If the TENSC option (tension stiffening applied to concrete) is used, the response of the material models to increasing tension strains is governed by the following rules:

a) A linear elastic behavior is assumed for $\sigma<\sigma_t$ (σ_t = concrete tensile strength). In Fig. A.1, at the end of the first load step $\varepsilon=\varepsilon_1$; the corresponding stress is σ_1 and the initial tangent modulus (E_o) is used. This modulus is also used for the next step;

b) If during a load step, the tensile stress increases such that the specified tensile strength (σ_t) is exceeded, initially no correction is applied to this computed stress. In Fig. A.1 if during the second load step the strain is increased from ε_1 to ε_2, the new stress value is σ_2 (independent of the number of iterations performed), and this stress is not yet corrected for having exceeded σ_t. Furthermore, the initial value of the tangent modulus (E_o) is assumed to remain at (E_o) for the next load step also;

c) If in the next load step the strain is further increased, the corresponding stress is then computed on the unloading branch of

+the σ-ε diagram. In Fig. A.1 at step 3, ε is increased to ε_3 and the corresponding stress is σ_3. Due to the assumption $E=E_o$, however, the residual load is proportional to $\Delta\sigma=\sigma_3'-\sigma_3$. This residual load is now iterated out of the system. At the next stiffness update the tangent modulus will be set to zero (in Fig. a.1, step 4, $\varepsilon=\varepsilon_4$ produced $\sigma=\sigma_4$).

The above behavior is controlled, in the material models, by the crack flags CFLAG and CCFLAG, with CFLAG = 0 corresponding to uncracked concrete, i.e., $\sigma<\sigma_t$, and CFLAG = 1 to cracked concrete. CFLAG is used to check the current state of the material and, consequently, to take decision, while CCFLAG is used to store the updated value of CFLAG. The updated value is transferred to CFLAG at iteration 1 of each next load step. In Fig. A.1, when $\sigma=\sigma_2$ (i.e., at the end of the second load step), CFLAG = 0 and CCFLAG = 1. As CFLAG = 0, the stress is computed by extrapolating along the linear branch of the diagram and the updated value for E will still be E_o. At the conclusion of the second step, CCFLAG is set to 1. Then in the next step, CFLAG is set to 1; if a stiffness update is requested (at the second iteration or further), E is set to zero.

As a consequence of this manner of handling the conditions at the initiation of cracking, the computed solution may depend on the load step size. An example is given in Fig. A.2a. The strain ε_b is reached through two load steps; the corresponding stress is σ_b. In Fig. A.2b the same strain ε_b is reached through three load steps, and the corresponding stress is σ_b'. Because the solution now includes enough load steps beyond

cracking to trigger iterations on the unbalanced excess tension, stress difference in final results are significant.

Due to the above problems, updating the tangent stiffness matrix at the second iteration, rather than at the first one, has been proven an efficient procedure.

2) If the TENSS option (tension stiffness lumped to steel) is used, the behavior of concrete is the same as with the TENSC option, while the steel stress is always given the corrected value, i.e., the most updated one. The global behavior at first cracking results to be as shown in Fig. A.3:

a) let the starting point be A, corresponding to a strain value ε_1;

b) if the strain is increased from ε_1 to ε_2', the new solution is not in B', as it might be expected, but, rather, in B, as the steel elastic modulus has been updated to the new value $4E_s$;

c) if no iteration is done, the solution at the next load step will be on the OD branch of the diagram, but,

d) if iterations are done, the negative residual load R_1 causes the strain to be reduced to a value ε_2''. This last corresponds to a positive residual load R_2. At the next iterations, the solution will always oscillate between strain values less than and greater than ε_t, respectively. No convergence can be found.

Choosing a suitable solution procedure

The above problems suggest that special care should be used in membrane applications, if one or both the material models are employed, and the TENSC option activated. Using a very small load step size could, generally, lead to a good solution, provided that a reduced number of iterations per step is done. While iterating, indeed, overshooting may occur at new integration points, and unloading will start at the next step only.

A more rational approach would require to size the load steps so as to minimize overshooting. This is what was tried in the present work; details about the solution procedure are given in the following. The procedure was applied to the shear wall elements, which undergo membrane stresses only.

For the purpose of checking whether overshooting occurred at an integration point, the tension principal stress has to be compared to the tensile concrete strength (σ_t). The output stresses come from the superposition of both concrete and steel stresses; so the concrete stresses have to be separated as:

$$\sigma_{x\text{-conc.}} = \sigma_{x\text{-tot.}} - \sigma_{x\text{-steel}} = \sigma_{x\text{-tot.}} - E_s \varepsilon_x$$

in each of the X and Y directions of the reference system. The principal strain directions have then to be found, which are assumed, in Milford's and Schnobrich's material model, to coincide with the principal stress directions. Finally, rotating the concrete stresses to the principal directions gives the "principal stresses". From these values, the σ-ε theoretical curve can be reproduced and cracking checked. The σ values for the current load step and the previous one are

now compared. If overshooting occurred at an integration point at a too large extent, comparing the two solutions suggests a better size for the load step, so as to reduce overshooting. If no new crack has opened, the size for the next load step is governed by the highest tension stress. After σ_t has been exceeded at an integration point, a small load step is used in order to allow a stiffness update.

A better solution to the problem, however, would require changes in the material model such that:

1) the computed solution is always on the σ-ε curve;
2) if cracking occurred, the tangent modulus is immediately set to zero (eliminate the need of waiting for a new load step).

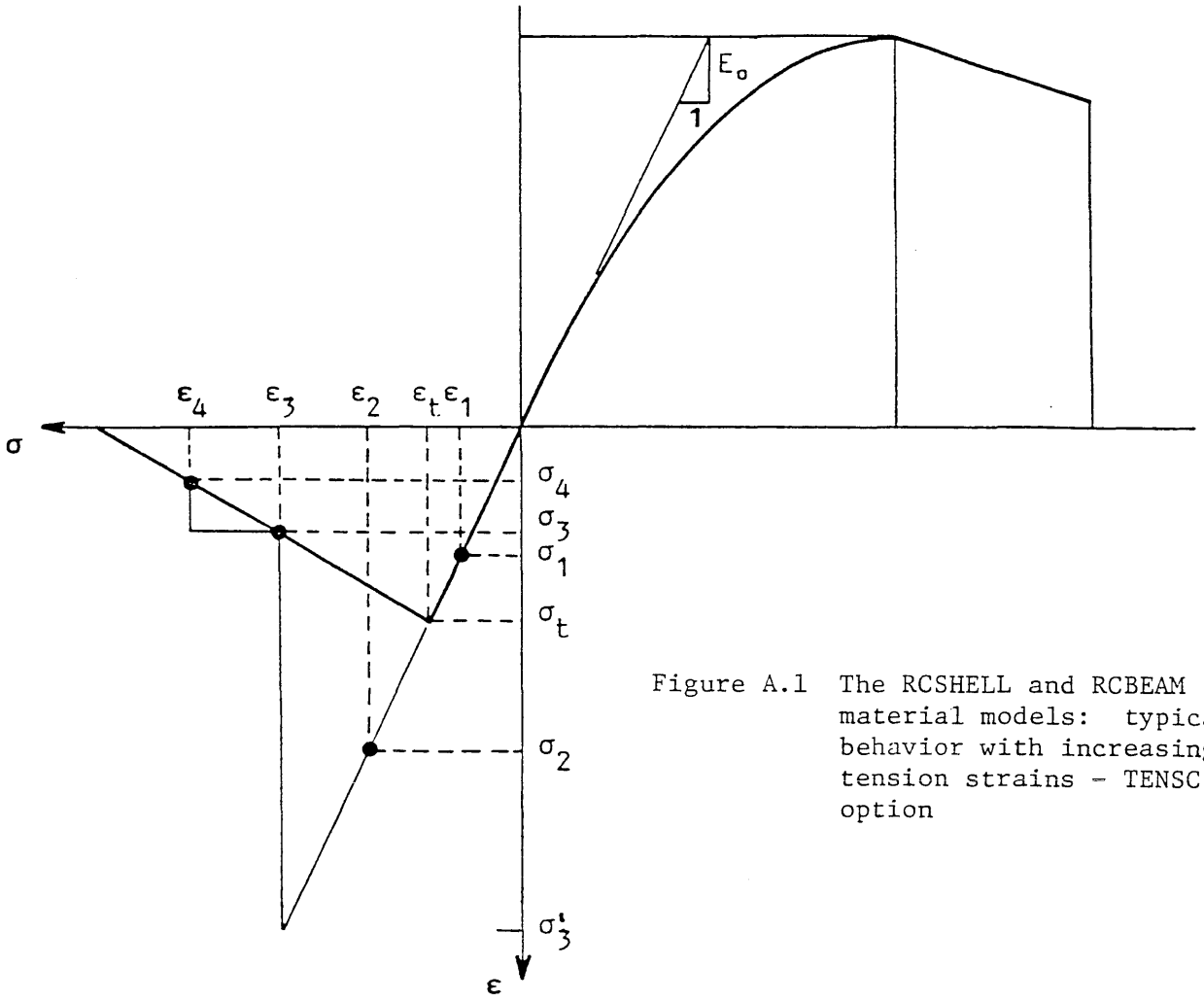

Figure A.1 The RCSHELL and RCBEAM material models: typical behavior with increasing tension strains - TENSC option

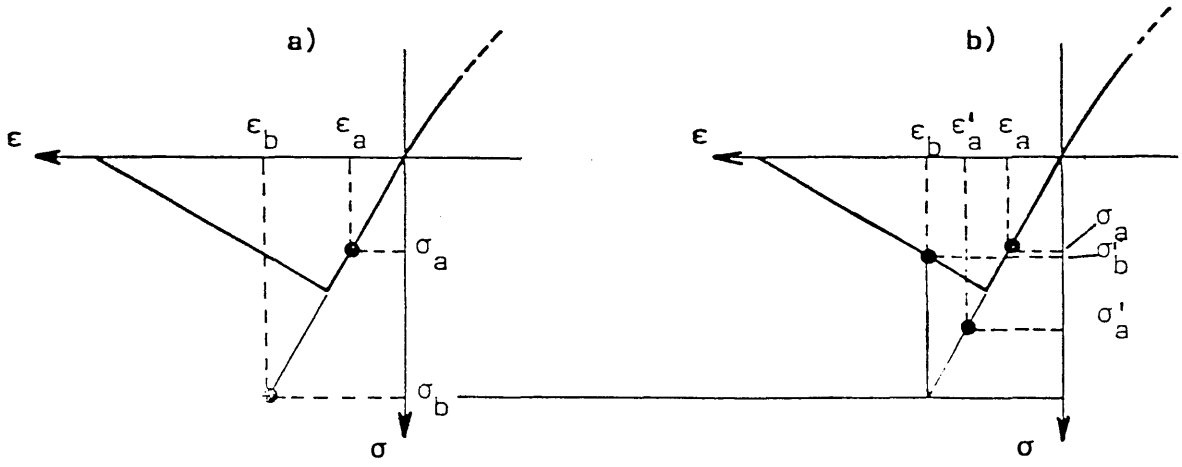

Figure A.2 Different responses due to different loading procedures

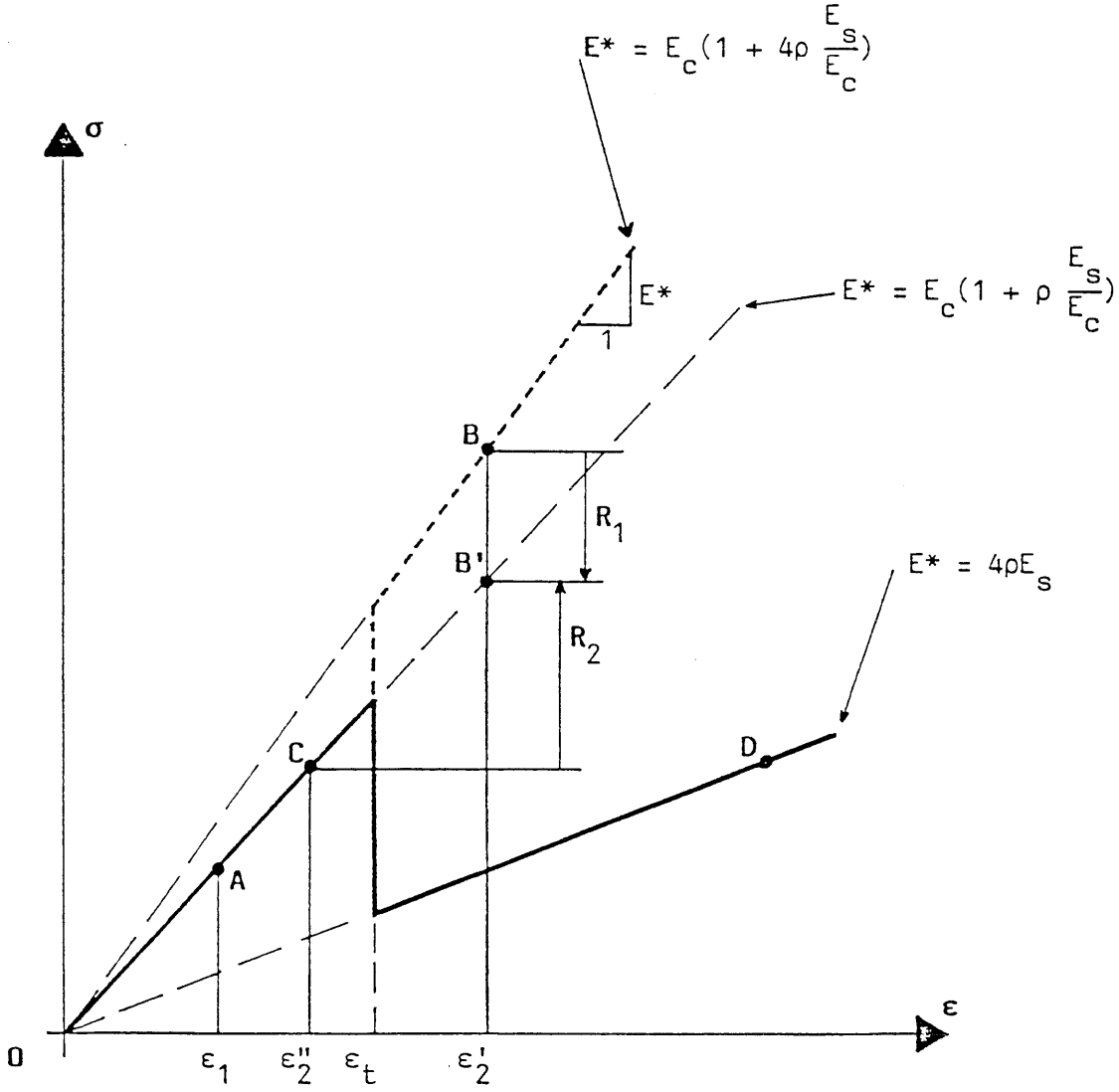

Figure A.3 Typical response with increasing tension strains - TENSS option

REFERENCES

1. Charney, F. A. and Bertero, V. V., "An Evaluation of the Design and Analytical Seismic Response of a Seven-Story Reinforced Concrete Frame-Wall Structure," Report no. UCB/EERC-82/08, University of California at Berkeley, California, August 1982.

2. Joglekar, M., Murry, P., Jirsa, J., and Klingner, R., "Full Scale Tests on Beam-Column Joints," in "Earthquake Effects on Reinforced Concrete Structures - U.S.-Japan Research," edited by James K. Wight, A.C.I. Special Publication no. SP-84, Detroit, 1985, pp. 271-304.

3. Milford, R. V. and Schnobrich, W. C., "Nonlinear Behavior of Reinforced Concrete Cooling Towers," Civil Engineering Studies, SRS no. 514, University of Illinois, Urbana, Illinois, May 1984.

4. Otani, S., Kabeyasawa, T., Shiohara, H., and Aoyama, H., "Analysis of the Full Scale Seven Story Reinforced Concrete Test Structure," in "Earthquake Effects on Reinforced Concrete Structures - U.S.-Japan Research," edited by James K. Wight, A.C.I. Special Publication no. SP-84, Detroit, 1985, pp. 203-240.

5. Wight, J., Bertero, V., and Aoyama, H., "Comparison Between the Reinforced Concrete Test Structure and Design Requirements from U.S. and Japanese Building Codes," in "Earthquake Effects on Reinforced Concrete Structures - U.S.-Japan Research," edited by James K. Wight, A.C.I. Special Publication no. SP-84, Detroit, 1985, pp. 73-104.

6. Yoshimura, M. and Kurose, Y., "Inelastic Behavior of the Building," in "Earthquake Effects on Reinforced Concrete Structures - U.S.-Japan Research," edited by James K. Wight, A.C.I. Special Publication no. SP-84, Detroit, 1985, pp. 163-202.